ChemComm

COMMUNICATION

View Article Online
View Journal | View Issue

Check for updates

Cite this: *Chem. Commun.*, 2024, **60**, 2946

Received 24th December 2023,
Accepted 14th February 2024

DOI: 10.1039/d3cc06248a

rsc.li/chemcomm

Open Access Article. Published on 14 February 2024. Downloaded on 6/12/2026 3:47:59 PM.
This article is licensed under a Creative Commons Attribution-NonCommercial 3.0 Unported Licence.

An aqueous alkaline zinc–sulfur flow battery†

Rui Nie,[a] Yizhe Nie,[a] Jiajun Wu,[a] Lihong Yu,*[b] Le Liu[a] and Jingyu Xi*[a]

We demonstrate a rechargeable aqueous alkaline zinc–sulfur flow battery that comprises environmental materials zinc and sulfur as negative and positive active species. Meanwhile, a nickel-based electrode is also obtained by a two-step process to decrease the polarization of the sulfur redox reaction, thus greatly improving the voltage efficiency of the system from 32% to 78% at 10 mA cm^{-2}.

Large-scale energy storage systems are widely demanded with the development of renewable energy.[1] Rechargeable batteries are one of the most important technologies for grid-scale energy storage (GES) applications by providing great operational flexibility.[2] There exist many types of rechargeable battery technologies and lithium-ion batteries (LIBs) occupy a major position in the battery market at present.[3] Despite LIBs having a high-energy density, using organic solutions and the overactive lithium metal cause safety problems, hindering their practical use in GES.[4] Aqueous batteries, especially aqueous zinc-metal batteries (AZMBs), are considered as an alternative of LIBs due to their inherent safety and high capacity, which has attracted tremendous research interest.[5]

Zinc (Zn) is an attractive material due to its low cost (2.9 US$ kg^{-1}), high theoretical capacity (819 mA h g^{-1}) and compatibility with aqueous electrolyte.[6] The early AZMBs used manganese-based, vanadium-based and organic-based cathodes with the conventional Zn^{2+} insertion/extraction mechanism.[7–9] Recently, conversion-type cathodes with multiple-electron transfers have replaced this traditional mechanism, promoting the capacity of AZMBs.[10,11] Sulfur (S) is the most representative cathode because of its high capacity (1675 mA h g^{-1}) and low cost of 0.25 US$ kg^{-1}.[10] Initial work with aqueous Zn–S primary batteries demonstrated an energy density of 1083.3 W h kg^{-1}.[12] However, when used in a rechargeable battery, this system exhibits significant polarization (more than 1.0 V) and a low discharge plateau of 0.3 V at a low rate, attributed to the sluggish kinetics of the S electrode.[13] Low discharge plateaus also exist in nickel-S, copper-S and lead-S batteries as reported.[14–16] Another reason which hinders the practical use is the formation of passivating ZnS.[17]

It has been demonstrated that charge carriers like lithium, sodium and potassium ions in aqueous electrolytes can benefit the kinetics of the S electrode and the performance of the full battery.[10,17] Flow batteries (FBs) would meet the requirement above.[18] The most attractive character of FBs is the design flexibility in decoupling power and energy, overcoming the issue of low discharge plateau of aqueous Zn–S batteries (AZSBs). The Zn–S couple has been tested in solid suspension flow batteries and only potential-current responses were displayed with no cycling performance.[19] The sluggish solid-to-solid phase transfer reaction of Zn, S and ZnS hinders the performance of cycling. Like polysulfide-iodide,[20] polysulfide-ferrocyanide,[21] polysulfide-permanganate[22] and S-manganese[23] FBs, using a cation-exchange membrane could make the Zn–S system rechargeable, avoiding the formation of ZnS at the same time.

Although the Zn–S battery, and Zn-based and S-based FBs have been widely developed, the Zn–S flow system has not been explored.[24] Herein, we demonstrate an aqueous alkaline Zn–S flow battery (AZSFB) for the first time. The active materials dissolved in alkaline solutions, rendering a discharge plateau of 0.5 V at 5 mA cm^{-2}. Meanwhile, a binder-free nickel-based electrode was prepared by a two-step process to improve the kinetics of the S redox reaction. The as-prepared electrode is composed of micro-nanosized defects and nickel oxide particles, which hugely decreases the polarization of the S redox reaction both in half-cell tests and FBs. Consequently, the voltage efficiency (VE) of the AZSFB using this positive electrode reached 78% at 10 mA cm^{-2}, almost twice that using the pristine graphene felt (GF) electrode. With low cost and high theoretical capacity, this AZSFB has great potential for further study.

Before constructing a new system FB, cyclic voltammetry (CV) was performed to test the redox potential of the active

[a] *Institute of Materials Research, Tsinghua Shenzhen International Graduate School, Tsinghua University, Shenzhen 518055, China. E-mail: xijy@tsinghua.edu.cn*
[b] *School of Materials and Environmental Engineering, Shenzhen Polytechnic University, Shenzhen 518055, China. E-mail: yulihong@szpt.edu.cn*

† Electronic supplementary information (ESI) available. See DOI: https://doi.org/10.1039/d3cc06248a

This journal is © The Royal Society of Chemistry 2024

Open Access Article. Published on 14 February 2024. Downloaded on 6/12/2026 3:47:59 PM.
This article is licensed under a Creative Commons Attribution-NonCommercial 3.0 Unported Licence.

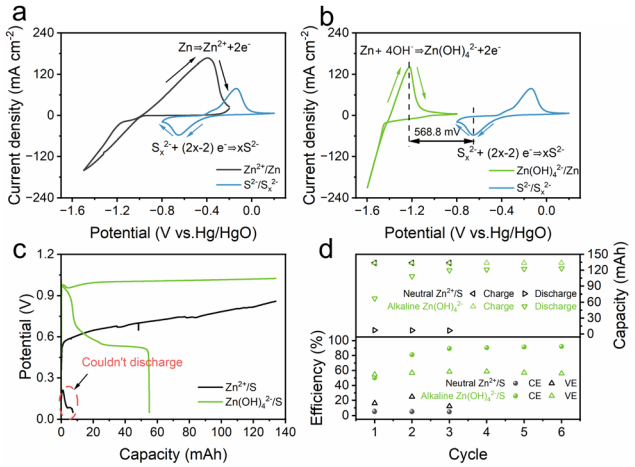

Fig. 1 (a) CV curves of $ZnSO_4$ in neutral solution and K_2S + KOH in alkaline solution. (b) CV curves of ZnO + KOH in alkaline solution and K_2S + KOH in alkaline solution. (c) Comparison of the charge/discharge curves of AZSFBs using $ZnSO_4$ and ZnO + KOH as the negolyte. (d) Cycling performance of AZSFBs using $ZnSO_4$ and ZnO + KOH as the negolyte. The upper part is the charge/discharge capacity and the lower part is the efficiency of two types of AZSFBs.

materials first, which could determine whether the redox couples could work as a full battery. The marked peaks in Fig. 1a and b represent the reaction and potential range of half-cells during the discharge process. Fig. 1a shows the CV curves of Zn^{2+} in neutral solution and S^{2-} in the alkaline solution (3 M KOH). The potential ranges of Zn oxidation and polysulfide (S_x^{2-}) reduction are overlapped, which means that the full battery constructed by these active materials under this chemical environment could not discharge. Changing the pH of the solution containing zinc ions is commonly used to decrease the redox potential.[25,26] Obviously, the redox potential of $Zn(OH)_4^{2-}$/Zn in an alkaline solution (3 M KOH) is more negative than that in a neutral solution (Fig. 1b) and there's a potential gap of 568.8 mV between the peak of Zn oxidation and the peak representing S_x^{2-} reduction. To further demonstrate the feasibility, AZSFBs with different negolytes were assembled. Fig. 1c depicts the charge/discharge curves of the AZSFBs using neutral and alkaline negolytes. As CV revealed above, the AZSFB with the alkaline negolyte could discharge while the voltage of the AZSFB with the neutral negolyte decreased quickly with a limited discharge capacity. The cycling performance shows that the ZSFB with the neutral negolyte failed after the third cycle at 5 mA cm^{-2} and the AZSFB with the alkaline negolyte could run stably (Fig. 1d). The discharge capacity and coulombic efficiency (CE) of the AZSFB gradually increased, reaching 120 mA h and 91% after three cycles. The higher discharge capacity and rechargeable characteristic results from the more negative potential of $Zn(OH)_4^{2-}$/Zn in alkaline solution.

Although the AZSFB with alkaline negolyte is rechargeable, the value of VE is under 60% even at a low current density of 5 mA cm^{-2}. It could be known from CV that S has a sluggish kinetics with a peak potential separation of 512.1 mV (Fig. 1b), which causes the low VE of the AZSFB. Therefore, it is necessary to improve the electrochemical characteristics of S for achieving better cycling performance in the full battery. Nickel-based materials are good catalysts for the S redox reaction in metal-S batteries and widely used as the electrode of polysulfide-based FBs.[20,22,23,27–31] Hence, a binder-free nickel oxide on GF (NiO@GF) was prepared as Fig. 2a described. Scanning electron microscopy (SEM) images show that the pristine GF fibre is smooth with no defects (Fig. 2b) and its surface is fully covered by Ni-MOF nanosheets (Fig. 2c) after the solvothermal reaction. Then, Ni-MOF transforms into Ni-based nanoparticles (NiO@GF-600) while annealing at 600 °C in an Ar atmosphere (Fig. 2d). It is verified by energy dispersive X-ray spectroscopy (EDS) that this nanoparticle is composed of element Ni, carbon and oxygen (Fig. S1, ESI†). Ni-MOF@GF annealed at 900 °C (NiO@GF-900) was also prepared as a comparison. The nanoparticles also exist on the surface of NiO@GF-900 (Fig. S2, ESI†). In more detail, the morphology of the nanoparticles in NiO@GF-600 is irregular with some defects on the surface of the GF fibre, while there is a spherical-like morphology in NiO@GF-900 and the defects change into micro-nano pores, as shown in Fig. S3 (ESI†). Furthermore, X-ray diffraction (XRD) was used to determine the difference of surface structure between the obtained materials at different temperatures (Fig. 2e). The XRD patterns show that the chemical composition of the nanoparticles obtained at 600 °C is NiO. With the

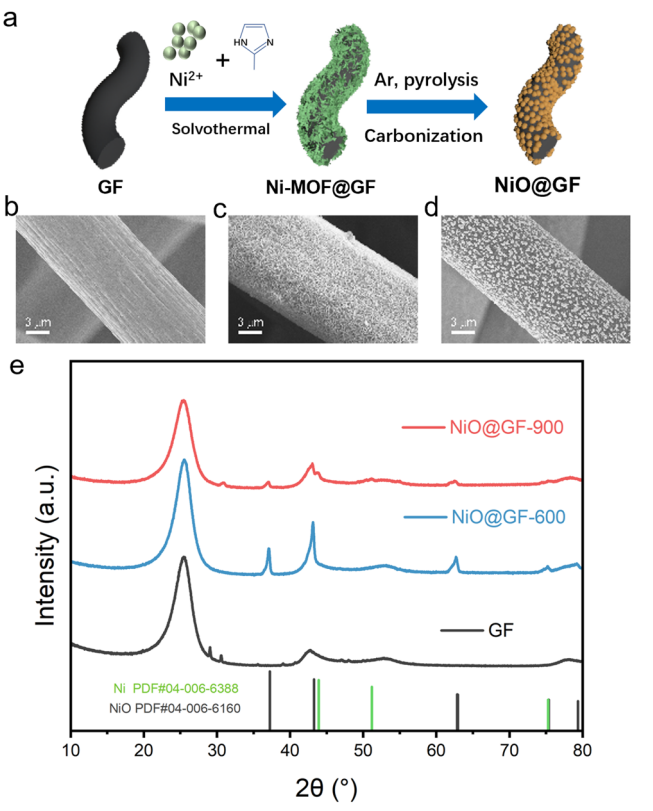

Fig. 2 Preparation and characterizations of the NiO@GF electrode. (a) Fabrication process of NiO@GF. (b–d) SEM images of (b) pristine GF, (c) Ni-MOF@GF and (d) NiO@GF-600. (e) XRD patterns of GF, NiO@GF-600 and NiO@GF-900.

Open Access Article. Published on 14 February 2024. Downloaded on 6/12/2026 3:47:59 PM.
This article is licensed under a Creative Commons Attribution-NonCommercial 3.0 Unported Licence.

temperature increased (900 °C), some of the NiO particles were reduced to metal Ni by carbothermal reduction reaction.[32]

Fig. 3 shows the electrochemical characterizations of the GF and NiO@GF electrode in the posolyte in a three-electrode configuration. As depicted in Fig. 3a, all electrodes have catalysis for S^{2-}/S_x^{2-} conversion. It is noteworthy that the CV curve of NiO@GF-600 shows higher current density and lower peak potential separation than the other two electrodes, which means faster redox reaction kinetics. CV curves in 3 M KOH were also tested to determine whether the electrodes themselves would react in alkaline solution (Fig. S4, ESI†). Only a small current density is observed, which means that the influence of the Ni redox reaction could be ignored. What's more, a smaller Tafel slope for the S_x^{2-} reduction reaction could be obtained from NiO@GF-600, delivering a lower voltage polarization (Fig. 3b). The faster kinetics of NiO@GF-600 is further supported by the electrochemical impedance spectroscopy (EIS) in Fig. 3c. The ohmic resistance (R_b) and charge transfer resistance (R_{ct}) of each electrode tested in the posolyte are summarized in Fig. S5 (ESI†). With a negligible change of R_b, the Nyquist plot of NiO@GF-600 demonstrates a much smaller semicircle, which means a smaller R_{ct} (2.6 Ω) than GF (14.1 Ω) and NiO@GF-900 (11.9 Ω). Depending on the result, NiO@GF-600 was chosen for further testing. Fig. 3d shows the CV curves at different scan rates using GF as a positive electrode. Despite the peak current density increasing with the scan rate increasing, the reduction peak shifted to the negative potential, finally out of the testing range. On the contrary, NiO@GF-600 shows better performance under the same test, and all peaks could be observed in the testing range at different scan rates, which demonstrates lower polarization and better catalysis (Fig. 3e). Fig. 3f summaries the separation of the peak potential (ΔE) with GF and NiO@GF-600 at different scan rates. The corresponding value of NiO@GF-600 is more than twice lower than that of GF. It could be predicted that using NiO@GF-600 as a positive electrode has a higher VE in AZSFB than GF.

Finally, AZSFBs were assembled to evaluate the effects of the NiO@GF-600 electrode in full batteries. Scheme and photograph of AZSFB are shown in Fig. 4a and Fig. S6 (ESI†), respectively. Negolyte and posolyte were pumped into the battery and reacted on the electrode. The preliminary experiment in Fig. 1d shows that the efficiency of AZSFB gradually improved for the first few cycles, so the system needs to be activated under low current density. AZSFB was activated at 5 mA cm^{-2} for three cycles, then cycled at 10 mA cm^{-2}. Fig. 4b shows the energy efficiency (EE) and VE of the AZSFB. The battery with GF as a positive electrode owns a stable VE at different current densities and EE increases gradually when activating then decreases at high current density. The value of VE is 32% and EE is 29% at 10 mA cm^{-2}. Using NiO@GF-600 could effectively improve the performance of the AZSFB. After activating, EE and VE still increase and become stable, demonstrating a higher value of EE (64%) and VE (78%). The discharge energy of the NiO@GF-600 based AZSFB is twice higher than that of GF (Fig. 4c). Charge/discharge curves of activating and cycling processes are also shown in Fig. S7 (ESI†) and Fig. 4d, respectively. The charge voltage is lower and the discharge plateau is higher when using NiO@GF-600 as a positive electrode, indicating a much lower polarization. This result of the full battery test agrees well with the CV results. It should also be noted that the coulombic efficiency of AZSFBs is only 91% at

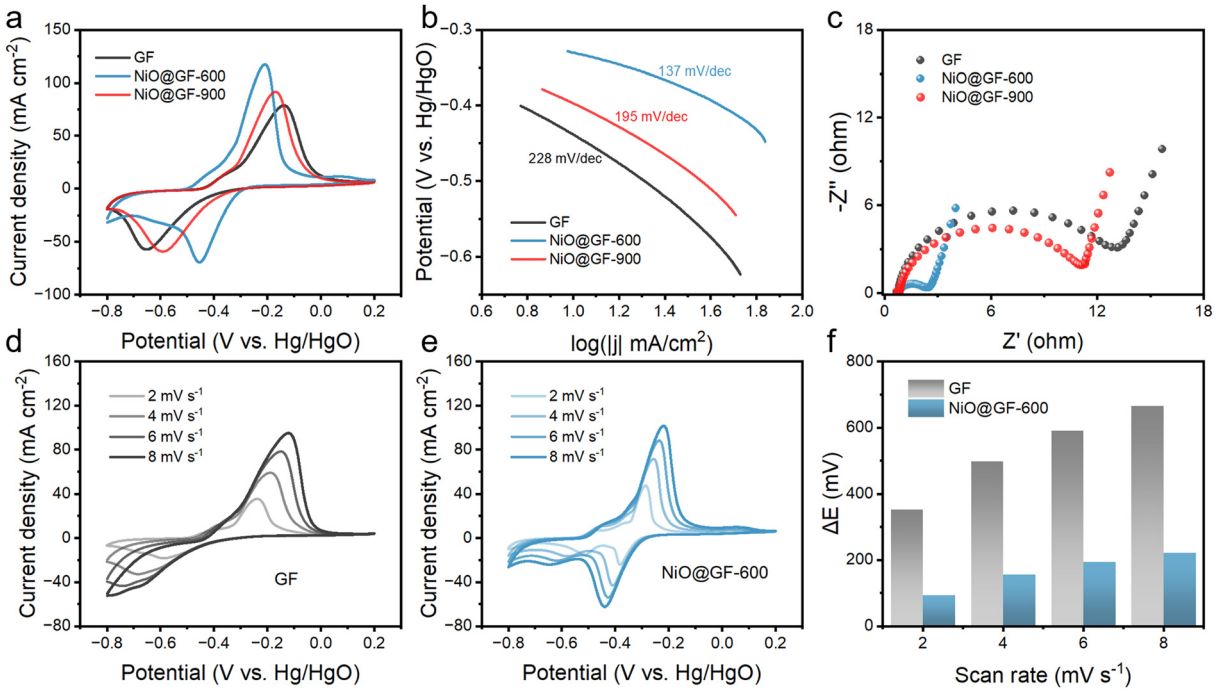

Fig. 3 Electrochemical performance of GF and NiO@GF in 0.1 M K_2S + 3 M KOH electrolyte. (a) CV curves of different electrodes at a scan rate of 10 mV s^{-1}. (b) Tafel plots for the corresponding reduction reaction in (a). (c) EIS spectra of different electrodes. CVs of (d) GF and (e) NiO@GF-600 at different scan rates. (f) Summary and comparison of the peak potential separation in (d) and (e).

 This journal is © The Royal Society of Chemistry 2024

Open Access Article. Published on 14 February 2024. Downloaded on 6/12/2026 3:47:59 PM.
This article is licensed under a Creative Commons Attribution-NonCommercial 3.0 Unported Licence.

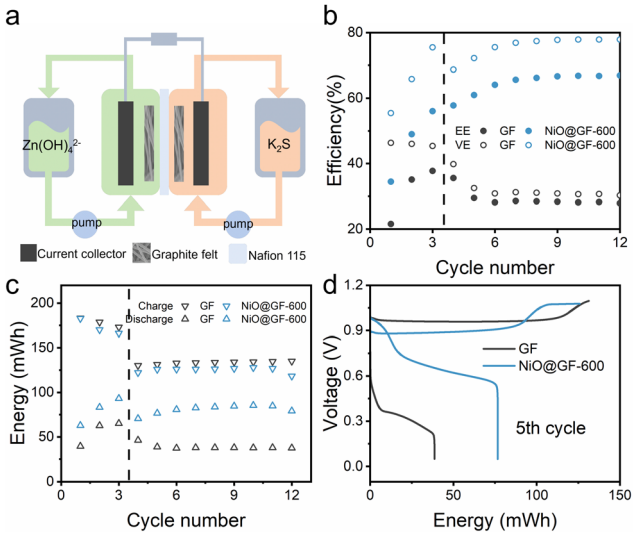

Fig. 4 Cycling performance of the AZSFBs with GF and NiO@GF-600 as positive electrodes. (a) Scheme of the AZSFBs. (b) Efficiencies and (c) charge/discharge energy of the AZSFBs with different positive electrodes. (d) Charge/discharge curves of the battery at the 5th cycle.

10 mA cm^{-2} (Fig. S8a, ESI†). The discharge capacity could only maintain a few cycles even if the charging process is limited by the capacity (Fig. S8b, ESI†). This is related to the membrane in S-based flow batteries. S_x^{2-} would crossover the Nafion membrane, causing the fast decrease of the active materials.[20] Although using two membranes like N115/N117 could slow down the cross-contamination, the low ion-selectivity of Nafion membrane is not effective to extend the cycle life of S-based flow batteries.[30] We are exploring the low-cost sulfonated poly(ether ether ketone) membrane and modifying this membrane to improve the ion-selectivity and inhibit the crossover of polysulfides, extending the cycle life of AZSFBs. These interesting results will be reported in the future.

In summary, we constructed an AZSFB successfully and prepared a NiO@GF-600 positive electrode to improve the performance. Using an alkaline solution could expand the voltage gap of the half reactions, making the system rechargeable. The prepared NiO@GF-600 electrode improves the peak current density and decreases the separation of peak potential of the S redox reaction, demonstrating a lower polarization. The assembled AZSFB with a NiO@GF-600 positive electrode shows higher discharge energy and more than twice higher EE and VE than GF. This work provides an example of designing a new type of FB system, enriching the family of low-cost aqueous flow batteries.

The authors appreciate financial support from the Natural Science Foundation of Guangdong Province (2022A1515011999) and the Shenzhen Basic Research Project (20200829101039001 and GXWD20201231165806004).

Conflicts of interest

There are no conflicts to declare.

Notes and references

1 Y. C. S. Chu and N. Liu, *Nat. Mater.*, 2017, **16**, 16–22.
2 W. Wang, B. Yuan, Q. Sun and R. Wennersten, *J. Energy Storage*, 2022, **52**, 104812.
3 H. Bai and Z. Song, *J. Power Sources*, 2023, **580**, 233426.
4 C. Han, Z. Li, W. Li, S. Chou and S. Dou, *J. Mater. Chem. A*, 2014, **2**, 11683–11690.
5 Y. Liu, X. Lu, F. Lai, T. Liu, P. R. Shearing, I. P. Parkin, G. He and D. J. L. Brett, *Joule*, 2021, **5**, 2845–2903.
6 W. Lu, C. Zhang, H. Zhang and X. Li, *ACS Energy Lett.*, 2021, **6**, 2765–2785.
7 H. Yang, D. Chen, R. Zhao, G. Li, H. Xu, L. Li, X. Liu, G. Li, D. Chao and W. Han, *Energy Environ. Sci.*, 2023, **16**, 2709–3168.
8 T. Wang, Y. Tang, M. Yu, B. Lu, X. Zhang and J. Zhou, *Adv. Funct. Mater.*, 2023, **33**, 2306101.
9 Y. Deng, R. Liang, G. Jiang, Y. Jiang, A. Yu and Z. Chen, *ACS Energy Lett.*, 2020, **5**, 1665–1675.
10 X. Wang, L. Liu, Z. Hu, C. Peng, C. Han and W. Li, *Adv. Energy Mater.*, 2023, **13**, 2302927–2302953.
11 D. Lin and Y. Li, *Adv. Mater.*, 2022, **34**, 2108856.
12 L. Luo, C. Zhang, X. Wu, C. Han, Y. Xu, X. Ji and J. Jiang, *Chem. Commun.*, 2021, **57**, 9918–9921.
13 W. Li, K. Wang and K. Jiang, *Adv. Sci.*, 2020, **7**, 2000761.
14 Z. Yang, B. Wang, Y. Chen, W. Zhou, H. Li, R. Zhao, X. Li, T. Zhang, F. Bu, Z. Zhao, W. Li, D. Chao and D. Zhao, *Natl. Sci. Rev.*, 2022, **10**, nwac268.
15 X. Wu, A. Markir, L. Ma, Y. Xu, H. Jiang, D. P. Leonard, W. Shin, T. Wu, J. Lu and X. Ji, *Angew. Chem., Int. Ed.*, 2019, **58**, 12640–12645.
16 C. Xu, Z. Yang, H. Yan, J. Li, H. Yu, L. Zhang and J. Shu, *Proc. Natl. Acad. Sci.*, 2022, **119**, e2118675119.
17 M. M. Gross and A. Manthiram, *ACS Appl. Mater. Interfaces*, 2018, **10**, 10612–10617.
18 L. Zhang, R. Feng, W. Wang and G. Yu, *Nat. Rev. Chem.*, 2022, **6**, 524–543.
19 S. Mubeen, Y. S. Jun, J. Lee and E. W. McFarland, *ACS Appl. Mater. Interfaces*, 2016, **8**, 1759–1765.
20 Z. Li, G. Weng, Q. Zou, G. Cong and Y. Lu, *Nano Energy*, 2016, **30**, 283–292.
21 B. Chen, H. Huang, J. Lin, K. Zhu, L. Yang, X. Wang and J. Chen, *Adv. Sci.*, 2023, **10**, 2206949.
22 M. Ding, H. Fu, X. Lou, M. He, B. Chen, Z. Han, S. Chu, B. Lu, G. Zhou and C. Jia, *ACS Nano*, 2023, **17**, 16252–16263.
23 J. Lei, Y. Yao, Y. Huang and Y. Lu, *ACS Energy Lett.*, 2023, **8**, 429–435.
24 Q. Y. Zhao, G. Y. Yin, Y. F. Liu, R. R. Tang, X. W. Wu and X. X. Zeng, *Carbon Neutralization*, 2023, **2**, 90–114.
25 J. Zhang, G. Jiang, P. Xu, A. Ghorbani Kashkooli, M. Mousavi, A. Yu and Z. Chen, *Energy Envir. Sci.*, 2018, **11**, 2010–2015.
26 R. Thamizhselvan, R. Naresh, R. Sekar, M. Ulaganathan, V. G. Pol and P. Ragupathy, *J. Energy Storage*, 2023, **61**, 106622.
27 H. Zhang, J. Chen, Z. Li, Y. Peng, J. Xu and Y. Wang, *Adv. Funct. Mater.*, 2023, **33**, 2304433.
28 T. Zhao, Y. Ye, X. Peng, G. Divitini, H. K. Kim, C. Y. Lao, P. R. Coxon, K. Xi, Y. Liu, C. Ducati, R. Chen and R. V. Kumar, *Adv. Funct. Mater.*, 2016, **26**, 8418–8426.
29 P. Zuo, H. Zhang, M. He, Q. Li, Y. Ma, C. Du, X. Cheng, H. Huo, Y. Gao and G. Yin, *Carbon*, 2017, **122**, 635–642.
30 Z. Li and Y. Lu, *Nat. Energy*, 2021, **6**, 517–528.
31 J. Lei, Y. Zhang, Y. Yao, Y. Shi, K. L. Leung, J. Fan and Y. Lu, *Nat. Energy*, 2023, **8**, 1355–1364.
32 F. J. V. S. K. Sharma and P. L. Walker, *Carbon*, 1997, **35**, 535–541.